Tertiary and Quaternary Structures of Photoreactive Fe-Type Nitrile Hydratase from *Rhodococcus* sp. N-771: Roles of Hydration Water Molecules in Stabilizing the Structures and the Structural Origin of the Substrate Specificity of the Enzyme[†,‡]

Masayoshi Nakasako,*[,§] Masafumi Odaka,[||] Masafumi Yohda,[||] Naoshi Dohmae,[||] Koji Takio,[||] Nobuo Kamiya,[||] and Isao Endo*[,||]

Precursory Research for Embryonic Science and Technology (PRESTO), Japan Science and Technology Corporation (JST), and The Institute of Molecular and Cellular Biosciences, The University of Tokyo, Bunkyoku, Tokyo 113-0032, Japan, and The Institute of Physical and Chemical Research (RIKEN), Wako, Saitama 351-0198, Japan

Received November 19, 1998; Revised Manuscript Received June 1, 1999

ABSTRACT: The crystal structure analysis of the Fe-type nitrile hydratase from *Rhodococcus* sp. N-771 revealed the unique structure of the enzyme composed of the α- and β-subunits and the unprecedented structure of the non-heme iron active center [Nagashima, S., et al. (1998) *Nat. Struct. Biol. 5,* 347−351]. A number of hydration water molecules were identified both in the interior and at the exterior of the enzyme. The study presented here investigated the roles of the hydration water molecules in stabilizing the tertiary and the quaternary structures of the enzyme, based on the crystal structure and the results from a laser light scattering experiment for the enzyme in solution. Seventy-six hydration water molecules between the two subunits significantly contribute to the αβ heterodimer formation by making up the surface shape, forming extensive networks of hydrogen bonds, and moderating the surface charge of the β-subunit. In particular, 20 hydration water molecules form the extensive networks of hydrogen bonds stabilizing the unique structure of the active center. The amino acid residues hydrogen-bonded to those hydration water molecules are highly conserved among all known nitrile hydratases and even in the homologous enzyme, thiocyanate hydrolase, suggesting the structural conservation of the water molecules in the NHase family. The crystallographic asymmetric unit contained two heterodimers connected by 50 hydration water molecules. The heterotetramer formation in crystallization was clearly explained by the concentration-dependent aggregation state of NHase found in the light scattering measurement. The measurement proved that the dimer−tetramer equilibrium shifted toward the heterotetramer dominant state in the concentration range of 10^{-2}−1.0 mg/mL. In the tetramer dominant state, 50 water molecules likely glue the two heterodimers together as observed in the crystal structure. Because NHase exhibits a high abundance in bacterial cells, the result suggests that the heterotetramer is physiologically relevant. In addition, it was revealed that the substrate specificity of this enzyme, recognizing small aliphatic substrates rather than aromatic ones, came from the narrowness of the entrance channel from the bulk solvent to the active center. This finding may give a clue for changing the substrate specificity of the enzyme. Under the crystallization condition described here, one 1,4-dioxane molecule plugged the channel. Through spectroscopic and crystallographic experiments, we found that the molecule prevented the dissociation of the endogenous NO molecule from the active center even when the crystal was exposed to light.

Nitrile hydratase (NHase,[1] EC 4.2.1.84) is a soluble bacterial enzyme catalyzing the hydration of various nitrile compounds to their corresponding amides ($RCN + H_2O \rightarrow RCONH_2$) (*1*). NHases consist of two subunits (α- and β-subunits) having M_r values of ca. 23K (*1*). Their amino acid sequences are well conserved among all known NHases (*2*). Non-heme iron (Fe-type NHase) (*3*) or noncorrinoid cobalt atom (Co-type NHase) (*4*) chelating to the α-subunit forms the catalytic center of the enzyme. Some Fe-type NHases exhibit an extraordinary characteristic in that the activities of the enzymes are regulated by light both in vivo (*5*−*7*) and in vitro (*8*, *9*). The enzyme completely loses its catalytic activity (inactive state) during the aerobic incubation

[†] This work was supported in part by grants for the Biodesign Research, for the SR structural Biology Research Programs, and for Promotion of Research from RIKEN. This work was also supported by Grants-in-Aid for Scientific Research on Priority (10129234 and 09261243) from the Ministry of Education, Science, Sports and Culture of Japan.

[‡] This structure has been deposited in the Brookhaven Protein Data Bank under file name 2AHJ.

* To whom correspondence should be addressed. M.N.: The Institute of Molecular and Cellular Biosciences, The University of Tokyo, Bunkyoku, Tokyo 113-0032, Japan; telephone, (81)-3-5841-8493; fax, (81)-3-5841-8493; e-mail, nakasako@iam.u-tokyo.ac.jp. I.E.: Biochemical Systems Laboratory, The Institute of Physical and Chemical Research (RIKEN), Hirosawa 2-1, Wako, Saitama 351-0198, Japan; telephone, (81)-48-467-9311; fax, (81)-48-462-4658; e-mail, endo@cel.riken.go.jp.

[§] Japan Science and Technology Corp. and The University of Tokyo.

[||] The Institute of Physical and Chemical Research.

[1] Abbreviations: NHase, nitrile hydratase; NO, nitric oxide; rms, root-mean-square; SEC-MALLS, multiangle laser light scattering combined with size-exclusion chromatography; L-NHase, Co-type NHase with a low molecular weight from *Rhodococcus rhodochrous* J1; H-NHase, Co-type NHase with a high molecular weight from *Rhodococcus rhodochrous* J1.

10.1021/bi982753s CCC: $18.00 © 1999 American Chemical Society
Published on Web 07/13/1999

of cells in the dark, but immediately recovers the activity upon light irradiation (active state). To understand the mechanism of this photo-reactivation, various types of spectroscopic techniques have been applied for Fe-type NHases (*10*−*15*). In particular, the Fourier transform infrared and the resonance Raman measurements showed that binding and releasing of a nitric oxide (NO) molecule in the active center caused this photoreactivity (*13*, *14*).

Recently, the structure of the active center has been determined via X-ray crystal structure analysis of the enzyme in the inactive state at a resolution of 1.7 Å (*16*). The photoreactive catalytic center consists of the non-heme iron atom coordinated to the sulfur atoms from three cysteine residues (Cys109A, Cys112A, and Cys114A) and two amide nitrogen atoms in the main chain of Ser113A and Cys114A. In the inactive state, an endogenous NO molecule occupies the sixth coordination site. Two of the three cysteine residues are post-translationally modified into cysteinesulfinic ($CysSO_2$-112A) and -sulfenic acids (CysSO114A). The two oxygen atoms of the cysteinesulfenic and -sulfinic acids form a claw setting structure with the OG atom from Ser113A. These two modifications were verified by Fourier transform mass spectrometry against the peptide fragments containing the active center (*16*, *17*). The structure of the active center is suitable for persistently capturing an endogenous NO molecule.

The active center is located at the interface of the α- and β-subunits, which fold into unusual tertiary structures. Both the active center and the quaternary structure of the enzyme seem to be stabilized by hydration water molecules existing in the interior and at the exterior of the enzyme. Hydration water molecules buried in proteins or interfaces in macromolecular complexes are quite important for stabilizing the structures of them by extending networks of hydrogen bonds (*18*−*22*).

In this paper, we focused on the structural roles of hydration water molecules in stabilizing the higher-order structures of this enzyme, based on the crystal structure and the results from light scattering measurements. As a result, we found that the hydration water molecules work as glue for stably forming the αβ heterodimer, the catalytic center, and the $(\alpha\beta)_2$ heterotetramer. In addition, we describe the structure of the entrance channel from the bulk solvent to the active center and discuss the plausible cause of the substrate specificity of this enzyme. The results from this work provide a new insight into the structural basis for realizing the photo-reactivation of the Fe-type NHase and provide a clue for the biotechnological applications of the enzyme.

MATERIALS AND METHODS

Sample Preparation. The NHase in the inactive state was purified from *Rhodococcus* sp. N-771 cells as described previously with a slight modification (*23*). The purification and crystallization were performed under a dim red light or in the dark to avoid photoreactivation of the enzyme. In every step of the preparation, absorption spectra were recorded for the small aliquots of sample solutions to confirm that the enzymes in the samples remained in their inactive state. The UV-2100PC spectrophotometer (Shimadzu) was used throughout. Until now, we have not experienced any activation of the enzyme in the dark or under a dim red light.

Table 1: Statistics for the Collected Diffraction Data and the Refined Structural Models

	dark	light
Data Collection		
crystal size (μm^3)	250 × 250 × 300	500 × 500 × 500
lattice constants (Å)		
a	117.4	117.6
b	145.6	146.0
c	52.1	52.1
X-ray wavelength (Å)	1.0000	1.5418 (CuKα)
resolution (Å)	40.0−1.70	40.0−1.85
no. of reflections	371002	258269
no. of unique reflections	88965	75030
completeness (%)	90.0	96.7
$R_{merge}{}^I$ [$I > 1\sigma(I)$][a]	0.060 (0.256; 1.75−1.70 Å)	0.079 (0.295; 1.90−1.85 Å)
$I/\sigma(I)$	52.8 (6.3; 1.75−1.70 Å)	27.4 (3.2; 1.90−1.85 Å)
$R_{iso}{}^b$		0.23
Structure Refinement		
resolution (Å)	8.00−1.70	8.00−1.85
no. of reflections used [$F > 2\sigma(F)$]	84827	72705
R-factor	0.173	0.160
$R_{free}{}^c$	0.223	0.203
rms deviation from the ideal case[d]		
bond (Å)	0.009	0.009
angle (deg)	1.640	1.675

[a] $R_{merge}{}^I = \Sigma_h\Sigma_i|I_i(h) - \langle I(h)\rangle|/\Sigma_h\Sigma_i I_i(h)$, where $I_i(h)$ is the intensity of the *i*th observation of reflection *h*; $R = \Sigma_h|F_{obs}(h) - F_{calc}(h)|/\Sigma_h F_{obs}(h)$, where $F_{obs}(h)$ and $F_{calc}(h)$ are the observed and calculated structure factors of reflection *h*, respectively. The data processing for the data collected in the dark was described previously (*16*). [b] R_{iso} was defined by the following equation: $R_{iso} = \Sigma_h|F_{dark}(h) - F_{light}(h)|/\Sigma_h F_{dark}(h)$, where $F_{dark}(h)$ and $F_{light}(h)$ are the observed structure factors of reflection *h* under the dark and light conditions, respectively. [c] R_{free} (*52*) was calculated for 10% of the unique reflections, which were not used in the structure refinement throughout. [d] Root-mean-square (rms) deviations from ideal stereochemical geometry.

Crystallization of NHase. Crystals were obtained as described previously (*16*, *24*). A small amount of zinc ion and 2−3% (v/v) 1,4-dioxane molecules were required in the precipitant solution for producing high-quality crystals. In particular, the absence of 1,4-dioxane caused disorder along the crystallographic *c* axis of crystals and decreased the effective resolution in diffraction patterns. The crystals belonged to space group $P2_12_12$ with the lattice constants listed in Table 1. Two NHase αβ heterodimers [$(\alpha\beta)_2$ heterotetramer] were contained in an asymmetric unit.

The absorption spectra of NHase molecules composing the crystals were recorded for the NHase solution obtained after dissolving the crystals by adding a standard buffer solution containing 50 mM HEPES/KOH and 3% (w/v) 1,4-dioxane (pH 7.5).

Further Crystallographic Refinement of the Previous Structural Model Determined under the Dark Condition. The crystal structure of the enzyme in its inactive state was determined and refined at a resolution of 1.7 Å as reported previously (*16*). In the study presented here, further rounds of structure refinement and model building were carried out against the previous model (*16*) with X-plor (*25*) and turbo FRODO (BIO-GRAPHICS). The structural model was refined with the stereochemical parameters of Engh and Huber (*26*) and without constraints with respect to the noncrystallographic symmetry. The diffraction intensity data

used for the structure refinement were collected at BL-18B (*27*) of the Photon Factory under the dark condition (Table 1). The number of hydration water molecules identified in the difference Fourier maps increased to 821, and torsion angles in the side chain groups of several amino acid residues were corrected according to the omit difference Fourier maps.

Hydration Structure Analysis and Structural Comparison of NHases. A program FESTKOP (M. Nakasako, unpublished work) was used to analyze the hydrogen bond networks in the enzyme. To compare the structure of NHase between the active and inactive states, the coordinate of the NHase in the active state (*28*) was taken from the Brookhaven Protein Data Bank (*29*) (file name 1AHJ). The NHase in the active state is from *Rhodococcus* sp. R312, whose amino acid sequence (*30*) is identical with that of the NHase from *Rhodococcus* sp. N-771 (*31*) analyzed here. This NHase from *Rhodococcus* sp. R312 exhibited photoreactivity both in vivo (*7*) and in vitro (*9*) as well as that from *Rhodococcus* sp. N-771 (*5*, *8*).

Multiangle Laser Light Scattering Measurements. The aggregation state of NHase in solution was investigated by the multiangle laser light scattering method combined with size-exclusion chromatography (SEC-MALLS). The measurement system was composed of a multiangle laser light scattering photometer (DAWN-F, Wyatt Technology) and a differential refractive index detector (Shodex RI SE-61, Showa Denko) connected to two successive gel filtration columns [Shodex KW-804 and KW-803 (Showa Denko)]. The columns were equilibrated with a solution containing 50 mM HEPES/KOH and 20 mM *n*-butyric acid (pH 7.0). The system was run with a flow rate of 1.0 mL/min, and samples of 0.1−0.2 mL were injected into the columns for each measurement. Data were collected at 1 s intervals, corresponding to a volume slice of 16.7 μL. Data collection and analyses were performed using the program ASTRA (Wyatt Technology) (*32*).

Crystal Structure Analysis for NHase in the Crystal under Light Irradiation. The X-ray diffraction experiment for the crystal under light irradiation was performed at our laboratory. The R-axis IV system (Rigaku) was used with an X-ray generator (Ultrax18, Rigaku) and double-mirror focusing optics (Rigaku). The diffraction data were collected at 293 K, as a series of 1.0° oscillations per 10 min exposure at the crystal-to-detector distance of 120 mm. The evaluation of the diffraction intensity data was carried out using the DENZO (*33*) and SCALEPACK programs (*33*). The statistics of the diffraction data up to a resolution of 1.85 Å are shown in Table 1. The slight changes of the lattice constants were observed (Table 1), probably because of a radiant heat. As listed in Table 1, the R_{iso} value between the two data sets was 0.23 for the reflections between 20 and 1.85 Å. This result indicated that slight rotation and/or translation of NHase molecules was induced by heat from the light irradiation. Therefore, we carried out not the difference Fourier analysis but the structure refinements by using the diffraction data collected under the light condition and the structural model described above as the starting model. The final statistics of the model are summarized in Table 1. The root-mean square (rms) difference of CA atoms was less than 0.2 Å between the structural models under the dark and light conditions.

RESULTS

Overall Structure of the Enzyme. Figure 1A shows the structure of the $(\alpha\beta)_2$ heterotetramer of NHase in a crystallographic asymmetric unit. Among the 821 hydration water molecules identified around the tetramer, 14 molecules were buried in α-subunits, 152 stabilized the heterodimers at their interface, and 50 mediated the interaction between the two $\alpha\beta$ heterodimers in the asymmetric unit. The orientation of the $\alpha\beta$ heterodimers in the asymmetric unit was identical to that observed in the crystal of NHase from *Rhodococcus* sp. R312 (*28*).

The structure of the $\alpha\beta$ heterodimer is presented in Figure 1B. The α-subunit (203 amino acid residues) had a characteristic tertiary structure: the "arm" domain composed of two perpendicularly oriented α-helices in the N-terminal region and the "globular" domain formed by nine α-helices and four β-strands. The β-subunit (211 amino acid residues) folded into two separate globular domains (the "helix" and the "sheet" domains) and two extremely long loops (Figure 1B). The non-heme iron center (*16*) was located at the interface of the two subunits and was composed of amino acid residues from the α-subunit in the "claw setting" sequence motif, Cys-X-Leu-Cys-Ser-Cys (in the case described here, the sequence was Cys109A-Ser110A-Leu111A-Cys112A-Ser113A-Cys114A).

In both subunits, separate domains had only a few interactions with each other. In the β-subunit, the two long loops also had a few interactions with the other portions in the subunit. In contrast, the domains and loops in a subunit strongly interacted with those in the other subunit in the $\alpha\beta$ heterodimer. These findings suggested that the formation of the heterodimer was indispensable for stabilizing the structure of the two subunits. In addition, the "arm" domain of the α-subunit wrapped around the "helix" domain of the β-subunit, and the long loop in the N-terminal region of the β-subunit wrapped around the "globular" domain of the α-subunit. This complicated structure in the $\alpha\beta$ heterodimer suggested that the heterodimer formation was not a simple docking of the two subunits but a dynamic process.

The rms differences in the positions of CA atoms in the heterodimers were less than 0.3 Å between the dimers in a crystallographic asymmetric unit, and the average rms difference in the positions of CA atoms was 0.39 Å between this inactive enzyme and the active one (*28*). In addition, the thermal factors of the main chain atoms were nearly identical over all the residues between the two heterodimers in an asymmetric unit. These facts should be explained clearly by the fact that the $\alpha\beta$ heterodimer was very rigid.

The Distribution of Hydration Water Molecules at the Interface of the α- and the β-Subunits. In the heterodimer, ca. 3700 Å^2 of surface area of each subunit was used in the interface of the α- and β-subunits. In this structural model, 76 hydration water molecules mediated the intersubunit interactions. Because the surface shapes of both subunits were not complementary at the interface (Figure 2), several cavities remained there. Thirty of the 76 molecules filled the cavities (Figure 1B), and the distribution of the 30 molecules in the cavities was identical for the two $\alpha\beta$ heterodimers in an asymmetric unit. From the point of view of the surface shape, the hydration water molecules extended the molecular surface of the subunits to make up the inconsistency in their surface shape.

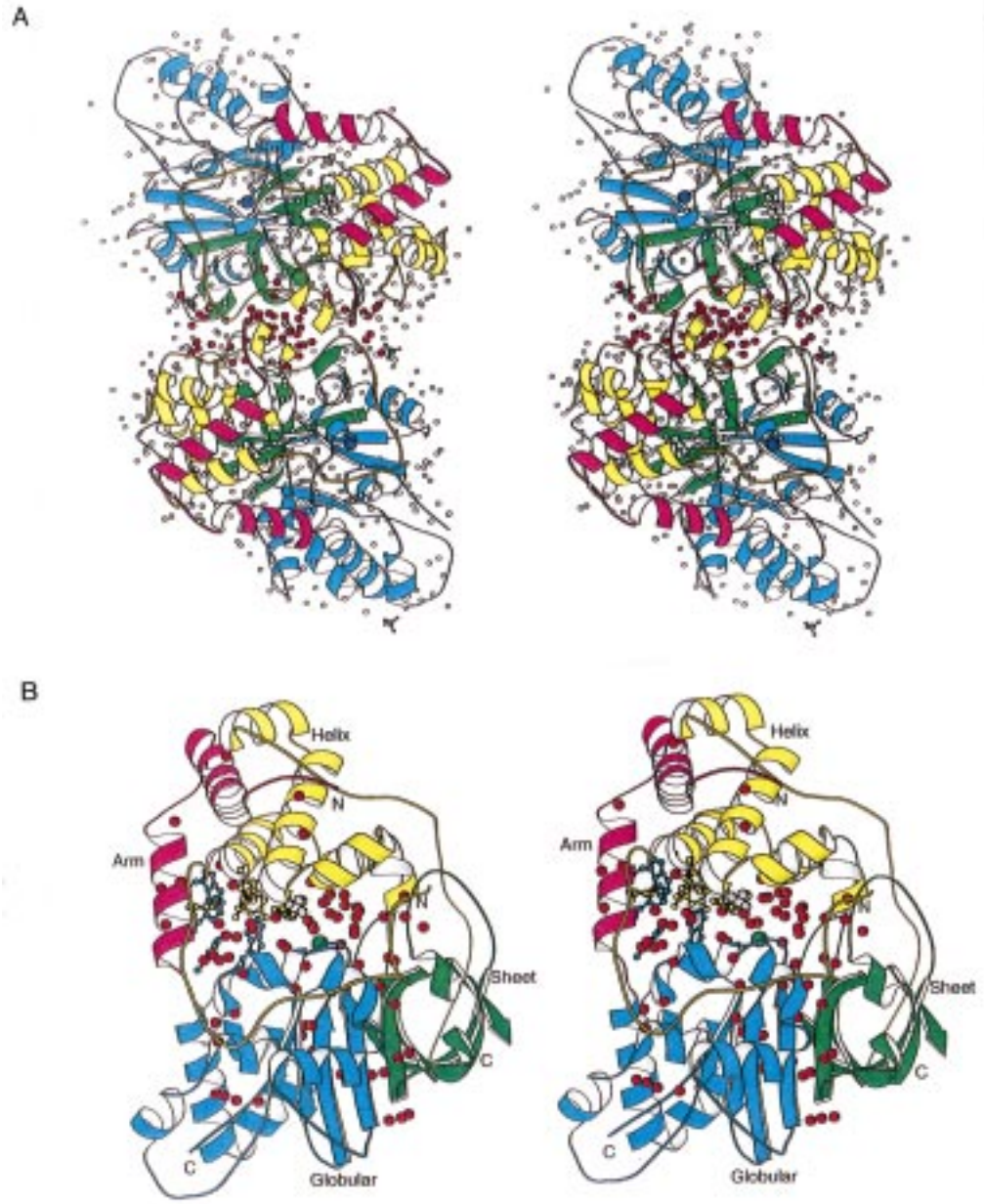

FIGURE 1: Stereoplots of ribbon diagrams for the quaternary structures of Fe-type NHase. The diagrams of the "arm" and "globular" domains in the α-subunits are red and cyan, respectively. In the *β*-subunit, the yellow structure is the "helix" domain, and the green structure is the "sheet" domain. Large green spheres denote the position of non-heme iron atoms. (A) The structure of $(\alpha\beta)_2$ heterotetramer with hydration water molecules in a crystallographic asymmetric unit. The red spheres are hydration water molecules mediating the interactions between the two *β*-subunits, and white spheres are the other hydration water molecules. Zinc ions and sulfate ions are represented as blue spheres and colored ball-and-stick models, respectively. The two 1,4-dioxane molecules are depicted with gray ball-and-stick models. (B) The structure of the α*β* heterodimer with hydration water molecules confined in the cavities between the two subunits. The hydration water molecules are depicted with red spheres. The ball-and-stick models represent 10 aromatic residues composing an aromatic cluster and a 1,4-dioxane molecule. This figure was prepared using MOLSCRIPT (*53*).

The hydration water molecules greatly contributed to the intersubunit interactions. Seventy-nine hydrogen bonds (<3.4 Å) were newly formed between the two subunits by the presence of the hydration water molecules, while 46 hydrogen bonds were identified between the α- and *β*-subunits alone. The contributions were observed not only for connecting the secondary structures of the subunits but also for stabilizing the loop structures. For instance, the long loop in the N-terminal region of the *β*-subunit interacted with the "arm" and "globular" domains of the α-subunit through 12 hydrogen bonds mediated by nine hydration water molecules.

In addition, the hydration water molecules were densely distributed on the negatively charged surface area of the *β*-subunit arising from a cluster of aspartic acids and glutamic acids from the "Helix" domain of the subunit. In particular, 10 hydration water molecules attached tightly to this negative surface. The surface of the α-subunit, which faced this negatively charged surface of the *β*-subunit, was electrostatically neutral (Figure 2A). Therefore, those hydration water molecules might have an important role in combining the two subunits with different electrostatic properties on their surfaces.

Hydration Water Molecules Stabilizing the Non-Heme Iron Active Center. The distribution of hydration water molecules at the interface was prominent around the active center; 20 hydration water molecules were densely distributed around

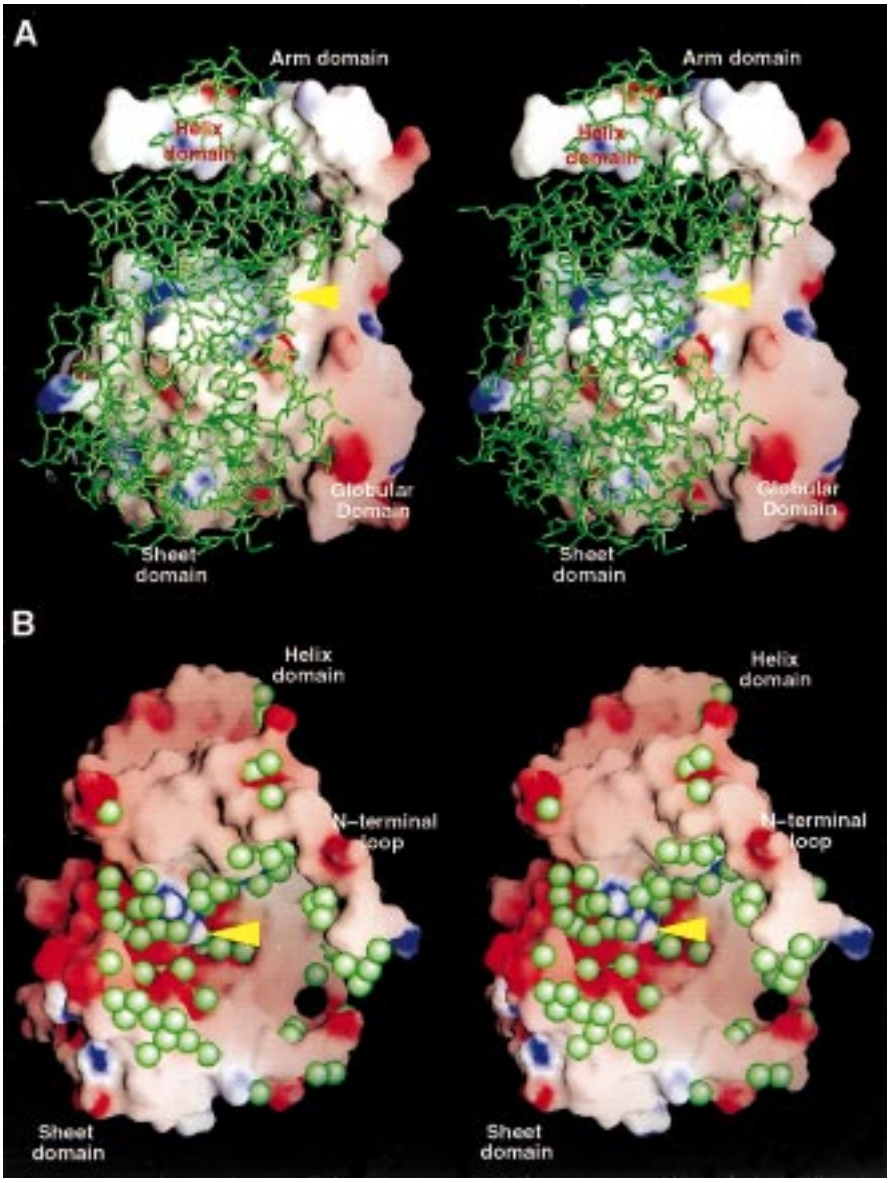

FIGURE 2: Stereoplots of the electrostatic potential at the molecular surface of the α- and *β*-subunits. The surface in red is negatively charged, and that in blue is positively charged. (A) The surface of the α-subunit with the stick model of the *β*-subunits in green. (B) The distribution of hydration water molecules on the surface of the *β*-subunit. The hydration water molecules shown here mediate intersubunit hydrogen bonds. The tips of the yellow arrows in both panels denote the position of the non-heme iron active center. These panels were prepared with GRASP (*54*).

the center (Figures 1B, 2B, and 3A). Networks of 57 hydrogen bonds were additionally formed at that interface around the center by the hydration water molecules (Figure 3), while only six direct hydrogen bonds were observed within protein atoms of the α- and *β*-subunits alone (Figure 3B). The thermal factor values of the hydration water molecules ranged between 10 and 25 Å^2, and the values highly correlated with those of the protein atoms hydrogen-bonded with the hydration water molecules. The small positional fluctuations of the hydration water molecules were advantageous in rigidly stabilizing the structure of the active center. These findings suggested that the structure of the active center was unstable without hydration water molecules.

The hydration water molecules around the active center were divided into three types with respect to the partner of their hydrogen bonds. (i) Three of them (2, 6, and 17 in Figure 3) directly interacted with the atoms in the active center. (ii) Four of them (5, 7, 13, and 14 in Figure 3) mediated hydrogen bond networks between the two subunits. (iii) Thirteen of them (1, 3, 4, 8−12, 15, 16, and 18−20 in Figure 3) stabilized the conformation of each subunit. Two hydration water molecules (6 and 17 in Figure 3) in the first group are likely to determine the conformation of the side chains of $CysSO_2$112A and Ser113A. Six hydration water molecules (8, 10−12, 14, and 19 in Figure 3) greatly contributed to neutralizing the negatively charged surface of the *β*-subunit (Figure 2B), as described above. Four of the third group (8, 10, 11, and 13 in Figure 3) fixed the conformation of the side chains of Arg141B and Arg56B, which directly stabilized the claw setting structure (Figure 3B) (*16*).

Interactions between the Two Heterodimers in the Crystalline State and the Aggregation State of NHase in Solution. At the interface of the two α*β* heterodimers in the $(\alpha\beta)_2$ heterotetramer, only three hydrogen bonds (<3.4 Å) and 12 van der Waals interactions (<4.0 Å) were found between

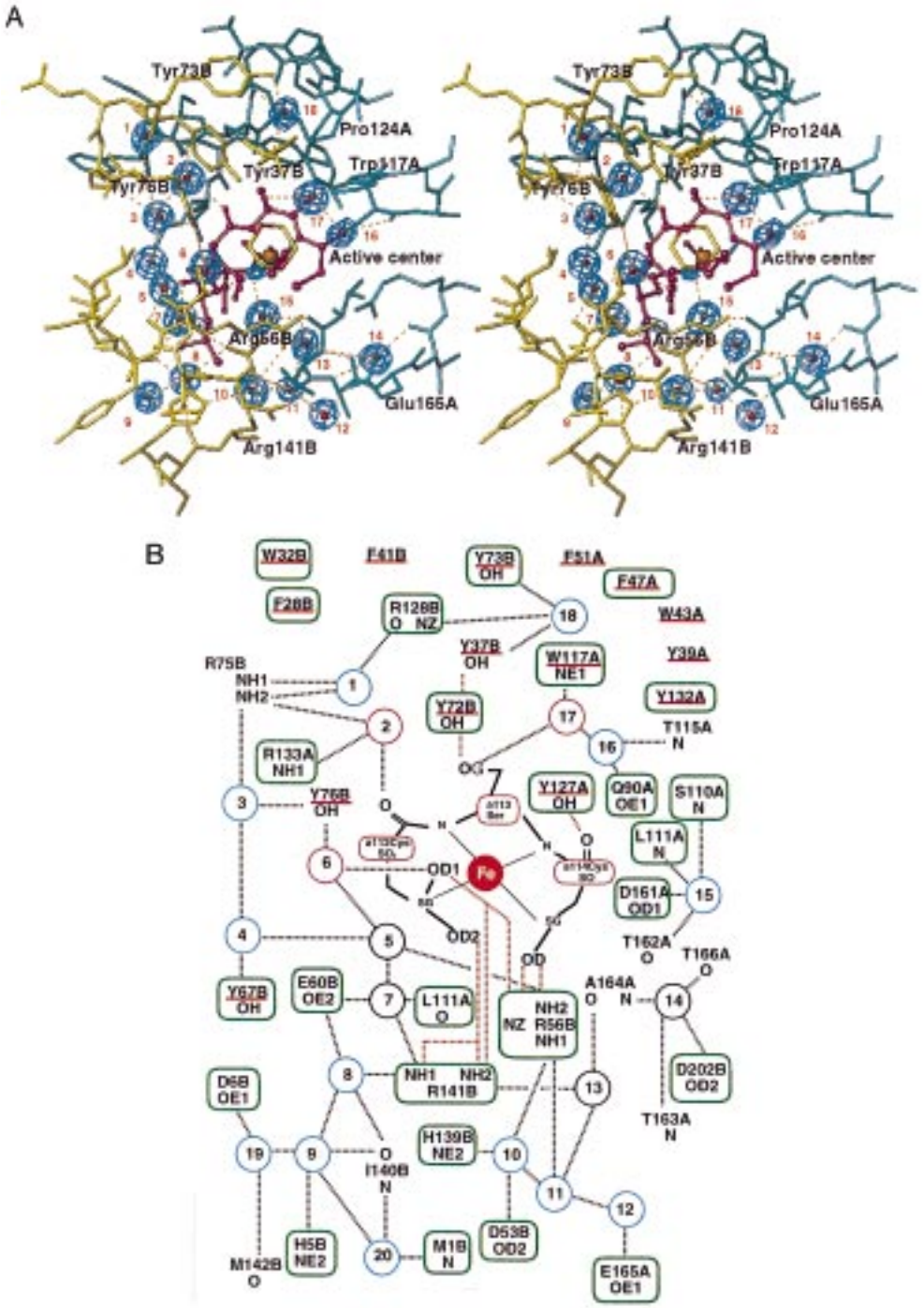

FIGURE 3: (A) Stereoplot of the ball-and-stick models for the structure around the non-heme iron active center, including 18 hydration water molecules. The residues in the α-subunit are cyan, and those in the β-subunit are yellow. The purple ball-and-stick model is the active center. The small red spheres denote the positions of hydration water molecules. The blue nets are the omit-annealed $F_o - F_c$ difference Fourier electron density maps for the hydration water molecules. The map is calculated with the reflections in the resolution range of 8.0−1.7 Å and is contoured at a 5.0 standard deviation level. The orange dashed lines represent possible hydrogen bonds between hydration water molecules and protein atoms. The hydration water molecules are numbered for clarity. (B) A schematic diagram for the extensive networks of hydrogen bonds formed around the active center. Possible hydrogen bonds are represented by dotted lines. The black dotted lines are hydrogen bonds formed between hydration water molecules and protein atoms, and the red ones are those between the polar protein atoms alone. Hydration water molecules are represented by circles. The figures in the circle correspond to the names of hydration water molecules defined in panel A. The colors of the circles correspond to the categories of hydration water molecules described in the text. The residues forming the active center are represented by red boxes. The residues with green boxes are conserved among six Fe-type and Co-type NHases (see Figure 7). Those underlined are the members of the aromatic cluster (see Figure 1B).

the two β-subunits. These interactions were not strong enough to maintain the quaternary structure of the heterotetramer of NHase. One of the reasons for this weak interaction was that the surface shape of the β-subunit was not complementary at the interface or in the case of the interface of the α- and β-subunits. However, the interdimer interaction was assisted by 50 hydration water molecules (Figure 1A). The molecules condensed into three separate regions and particularly stabilized the N-terminal and the second long loops in the β-subunits through hydrogen bonds.

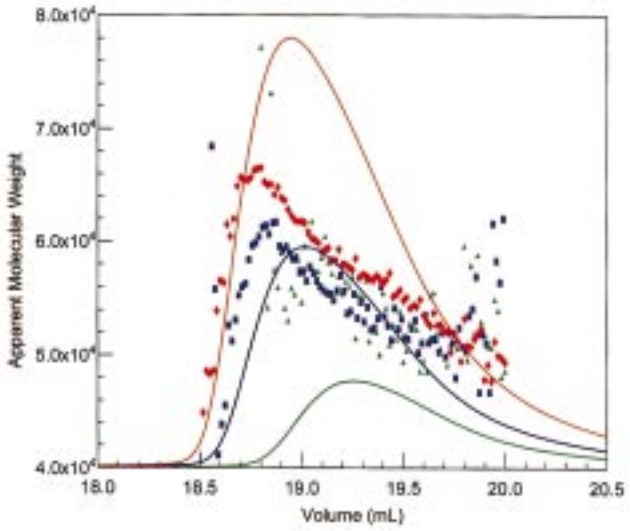

FIGURE 4: Plot of the apparent molecular weights of NHase vs elution volume in multiangle laser light scattering measurements. The symbols represent the apparent molecular weights estimated from a light scattering measurement against a slice with a 16.7 μL volume. The smooth curves are elution profiles from gel filtration columns. Curves (or symbols) in green, blue, and red are the results obtained for 40, 100, and 200 μg samples of photoactivated NHase, respectively.

The aggregation state and the minimum functional unit of this Fe-type NHase in solution were analyzed by SEC-MALLS against the NHase solution with different concentrations (Figure 4). In all samples, the enzyme eluted as a single peak with a large tail. The apparent molecular weight decreased from 66K to 51K, accompanying the elution volume in all conditions irrespective of the different elution profiles (Figure 4).

Although NHase in the inactive state existed as a heterotetramer [$(\alpha\beta)_2$, M_r = 92K] in the crystalline state, the variation in the apparent molecular weight indicated that NHases in solution were in an equilibrium between the $\alpha\beta$ heterodimer and the $(\alpha\beta)_2$ heterotetramer in the concentration range that was examined. The large tailing in elution profiles was explained by the fact that NHase heterodimers easily formed heterotetramers in the concentration range of 10^{-2}—1 mg/mL. The exchange rate in the equilibrium was considered to be so rapid that size-exclusion chromatography was not able to separate the heterodimers and -tetramers.

Structure of the Channel from the Bulk Solvent to the Active Center. The channel from bulk solvent to the active center was located at the interface of the α- and β-subunits (Figures 1B and 5). Five residues from the α-subunit (Gln90A, Glu92A, Trp117A, Glu165A, and Arg167A) and four hydrophobic residues from the β-subunit (Met40B, Phe41B, Val44B, and Val52B) directly formed the channel. In addition, the channel was partly stabilized by an aromatic cluster composed of 10 aromatic residues from the helix bundle of the "Arm" and "Helix" domains (Trp43A, Phe47A, Phe51A, Trp117A, Phe28B, Trp32B, Tyr37B, Phe41B, Tyr72B, and Tyr73B; Figure 1B). Six hydration water molecules engaged in forming hydrogen bond networks on the hydrophilic face of the channel.

The entrance of the channel formed by Gln90A, Phe41B, Val44B, and Val52B was ca. 10 Å from the active center. The entrance of the channel was too narrow (diameter of ca. 4 Å) for substrates, and only water molecules seemed to be able to pass through it. No significant structural changes were observed in the channel between this inactive state and the active states (*28*). Therefore, dynamical structural changes in those residues should occur to open and close the channel during the catalytic cycle.

Spectroscopic and Crystallographic Analysis of the NHase Crystal under Light Irradiation. The 1,4-dioxane molecule required for producing the high-quality crystals was found in the channel. The molecule was located 6 Å distant from the non-heme iron center and had 13 van der Waals interactions (<4.0 Å) with surrounding amino acid residues (Gln90A, Cys114A, Trp117A, Tyr37B, Met40B, Val52B, Arg56B, Tyr72B, and Tyr76B) (Figure 5). In particular, the endogenous NO molecule formed strong contacts with the 1,4-dioxane molecule (four van der Waals interactions). Because the molecular dimension of the 1,4-dioxane molecule was larger than the diameter of the entrance of the channel, the molecule seemed to reside in the channel and to prevent the dissociation of the endogenous NO molecule even under the light condition. To examine this possibility, we carried out absorption spectra measurements and structure analysis for a crystal under light irradiation.

Prior to the absorption spectra measurements, the crystals were set under light irradiation (5000 lx) for 15 min. Then, crystals were dissolved in the dark, and an absorption spectrum was measured. After the measurement, the solution was set under the same irradiation condition, and another absorption spectrum was measured. Under the dark condition, the spectrum had a shoulder at 370 nm, indicating that the NHase molecules in the solution still remained in their inactive state (Figure 6A). In contrast, after the light irradiation, the shoulder decreased and a small maximum appeared at 673 nm. The difference spectrum (Figure 6B) indicated that NHase molecules in the solution turned to their active state after the irradiation and that the molecules in the crystalline state were in their inactive state.

In addition, in the crystal structure of NHase under continuous light irradiation at 1000 lx (Table 1), the 1,4-dioxane molecule and an electron density above the non-heme iron center still remained (Figure 6C) as well as under the dark condition (*16*). The result from the absorption measurements and this crystal structure analysis indicated that the electron density above the center was the endogenous NO molecule and the molecule still bound to the center even under light irradiation because of the presence of the dioxane molecule.

We identified no significant positional differences in the coordination sphere of the active center greater than 0.2 Å around the active center between the light and the dark conditions (Table 2), except for the side chain of the post-translationally modified CysSO114A (Figure 6C). A peak in the $|F_o - F_c|$ difference Fourier map near the OD atom of CysSO114A suggested the possibility that the interaction between the OD atom and the NO molecule was broken up by the light irradiation. The detailed analysis of this possibility will be reported and discussed elsewhere with the structural model of the NHase in the active form solved at high resolution (Y. Kawano et al., manuscript in preparation).

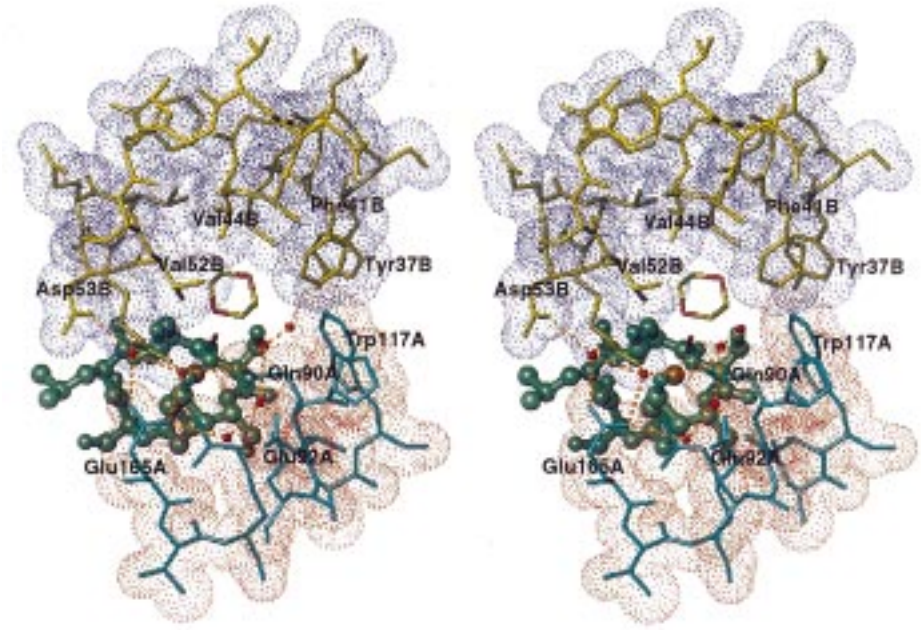

FIGURE 5: Stereoplot for the structure of the entrance channel from the bulk solvent to the active center viewed along the molecular axis of the endogenous NO molecule bound to the active center. The residues forming the channel are presented as stick models colored cyan for the α-subunit and yellow for the *β*-subunit. To visualize the size of the channel, van der Waals radii of protein atoms (shown with dots) are superimposed on the model. The green ball-and-stick model shows the active center. The 1,4-dioxane molecule interacting with the NO molecule and the six hydration water molecules (red spheres) bound to polar atoms are also shown. The orange dashed lines represent possible hydrogen bonds mediated by hydration water molecules.

Table 2: Distances between Atoms Composing the Non-Heme Iron Active Centers under the Dark and Light Conditions

	distance (Å)	
atom pair	dark[a]	light
Fe−N (NO)	1.65	1.66
Fe−SG (Cys109A)	2.30	2.25
Fe−SG ($CysSO_2$112A)	2.26	2.19
Fe−SG (CysSO114A)	2.33	2.30
Fe−N (Ser113A)	2.05	2.12
Fe−N (CysSO114A)	2.09	2.07
N(NO)−OD1 ($CysSO_2$112A)	2.92	2.91
N(NO)−OG (Ser113A)	2.95	3.04

[a] The bond distances under the dark condition were taken from the previous paper (*16*).

DISCUSSION

On the basis of the crystal structure of the Fe-type NHase in the inactive state, we analyzed the role of hydration water molecules in stabilizing the higher-order structures. Here, we discuss the biological implications of these results for the NHase family and the structure of the entrance channel likely causing the substrate specificity of the enzyme.

Roles of Hydration Water Molecules in the Association of the Two Subunits in Fe-Type NHase. In the heterodimer of this Fe-type NHase, the 30 hydration water molecules are confined in the cavities between the α- and *β*-subunits (Figures 1B, 2, and 3). The number of hydrogen bonds formed within the heterodimer was remarkably increased by the presence of the hydration water molecules, in particular, around the active center. In addition, according to the results from the systematic analysis of the cavities in a number of macromolecules (*34*), about one-third of the residues forming the cavities in NHase are disfavored in the formation of cavities (Arg56B, Arg75B, Arg128B, Arg141B, Glu165A, and Glu60B). This may be an exception from the point of view of the standard case (*34*). However, these residues tightly hydrogen-bonded to the hydration water molecules and engaged in the extension of the networks of hydrogen bonds stabilizing the active center. A number of hydration water molecules may enable this exceptional mode in cavity formation. These findings indicate that the hydration water molecules may be one of the key structural determinants responsible for the stable association of the two subunits and for maintaining the unique structure of the active center.

In the case of NHase, the electrostatic properties on the interfacial surface of the two subunits are quite different (Figure 2), and hydration water molecules are densely distributed on the negatively charged surface of the *β*-subunit (Figure 2B). This fact indicates that the hydration water molecules may assist energetically the association of the subunits. The orientational polarizability of water molecule is remarkably high in solution and is still significant even within protein molecules (*35*). This electrostatic property of hydration water molecule causes the solvent shielding effects contributing to the decrease in the free energy of the solvated system (*35*). Therefore, the hydration water molecules existing at the interface of NHase, in particular on the negatively charged surface of the *β*-subunit, may moderate the surface charge via their polarizability and decrease the free energy in the heterodimer association. In addition, electrostatic interactions between oppositely charged groups hinder binding (*36*), and this effect is understood because of the idea that the free energy costs of removing hydration water molecules are larger than those of forming electrostatic interactions (*37*). These two different electrostatic effects originated from hydration water molecules, and the protein itself may enable the association of the two subunits having different electrostatic properties at their surfaces.

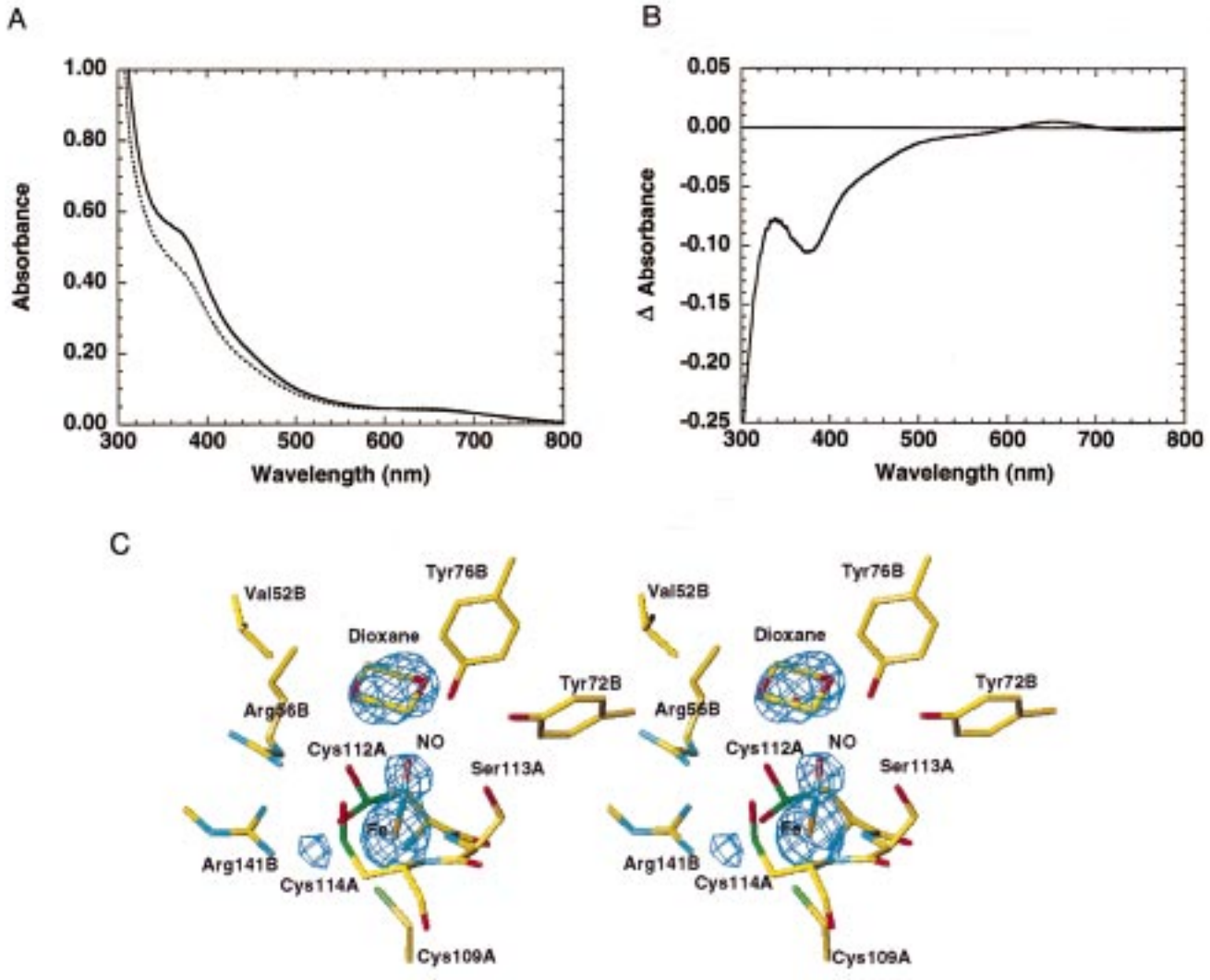

FIGURE 6: (A) Absorption spectra of the NHase solution obtained by dissolving the crystals. The solid line is the spectrum measured under the dark condition, and the dotted line is the spectrum measured after light irradiation of the solution. (B) Difference between the absorption spectra under the light and dark conditions. (C) A stereoplot of the ball-and-stick models for the structure of the active center under the light condition. The blue nets are the omit-annealed $F_o - F_c$ difference Fourier electron density maps for the non-heme iron atom, the endogenous NO molecule, and the 1,4-dioxane molecule. The map is calculated with the reflections in the resolution range of 8.0−1.85 Å and is contoured at a 5.0 standard deviation level.

The hydration water molecules in the interface produce a number of hydrogen bonds mediating the subunit−subunit interactions. Some of them extend specifically the networks of hydrogen bonds and significantly contribute to stabilizing the unique structure of the active center (Figure 3). As observed in macromolecular DNA−protein (*38*, *39*) and antigen−antibody complexes (*21*), water-mediated hydrogen bonds sometimes become the principal determinants in specifying the association of macromolecular complexes. In addition to those cases, the hydration water molecules in NHase may be structural determinants in the association of the two subunits. By the presence of the molecules, the enthalpic costs required in the formation of the heterodimer may be lowered as observed in several systems of macromolecular complexes (*40*).

In conclusion, the hydration water molecules in the subunit interface (i) extend the networks of hydrogen bonds connecting the two subunits, (ii) increase the complementarity of the surface shape of the two subunits, and (iii) moderate the electrostatic potential on the surface of the β-subunit. All these effects greatly decrease the enthalpic costs caused by the differences in the surface shapes and in the electrostatic properties of the surfaces of the subunits in the formation of the $\alpha\beta$ heterodimer.

Structural Importance of Hydration Water Molecules in Stabilizing the Active Center Structure of the NHase Family. Around the active center, the 20 hydration water molecules (Figure 3B) stabilize the conformation of the 17 amino acid residues (Gln90A, Ser110A, Leu111A, Trp117A, Asp161A, Glu165A, Asp6B, Asp53B, Arg56B, Glu60B, Tyr72B, Tyr73B, Arg128B, Arg133B, His139B, Arg141B, and Asp202B) highly conserved among all known Fe-type and Co-type NHases (Figure 7). When the sequence identity among Fe-type NHases (Figure 7) and the patterns in the extensive networks of hydrogen bonds are considered, the 20 hydration water molecules in Figure 3B should ubiquitously exist among Fe-type NHases. The importance of the hydrogen bond network is experimentally confirmed by our current mutagenesis experiments; a mutated enzyme having a smaller number of hydrogen bonds around the active center exhibits a drastic decrease of the enzymatic activity (S. Piersma et al., manuscript in preparation).

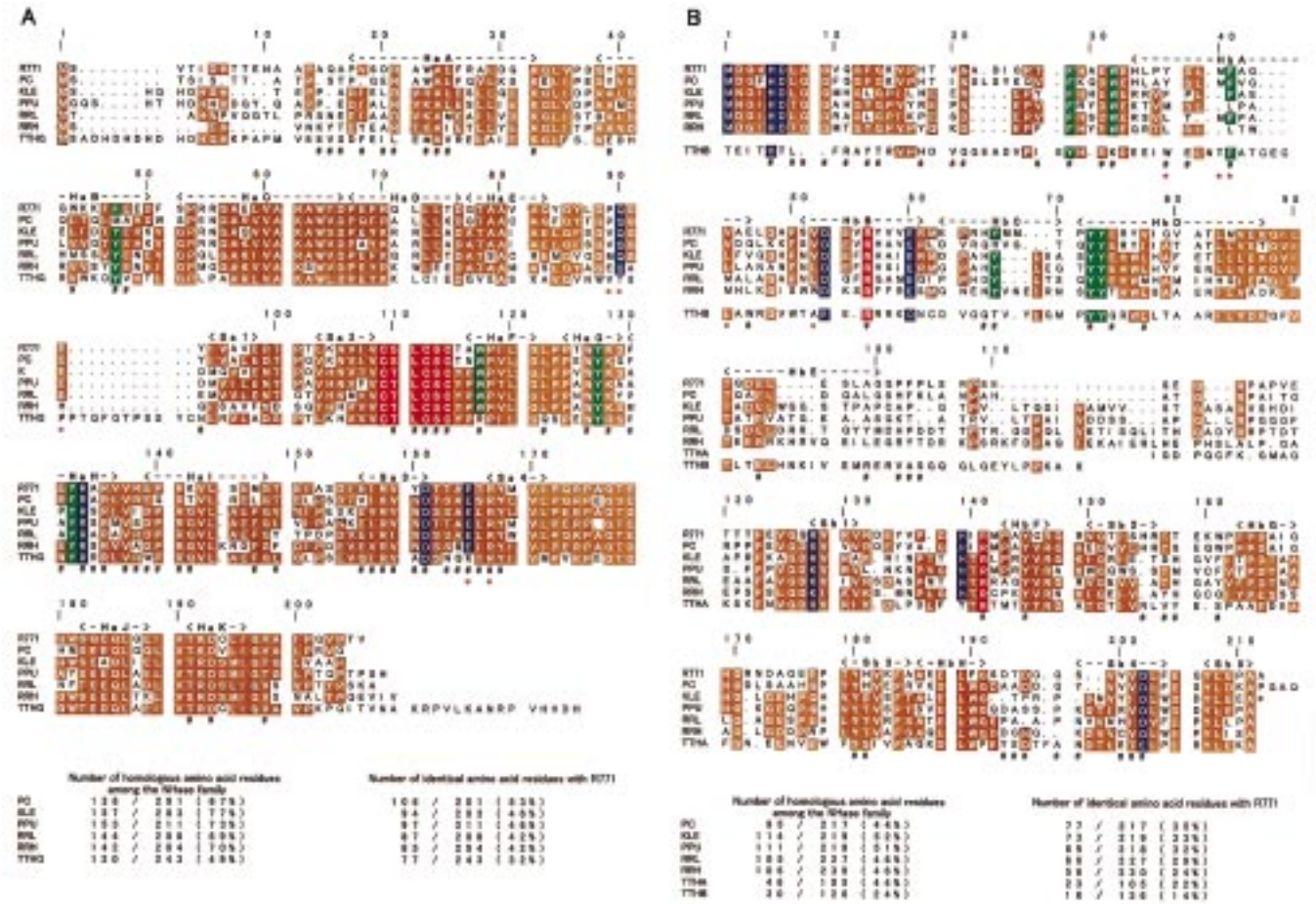

FIGURE 7: Amino acid sequence alignments of the α- and *β*-subunits of NHases and the α-, *β*-, and *γ*-subunits of thiocyanate hydrolase. The residue numbers are in accordance with those in Fe-type NHase from *Rhodococcus* sp. N-771. The NHases are as follows: R771, Fe-type NHases from *Rhodococcus* sp. N-771 (*31*), sp. N-774 (*44*), or sp. R-312 (*30*); PC, Fe-type NHase from *Pseudomonas chlororaphis* B23 (*55*); KLE, Co-type NHase from *Klebisiella* [GenBank (*56*) accession codes E08304 and E08305]; PPU, Co-type NHase from *Pseudomonas putida* (*57*); RRL, Co-type NHase with a low molecular weight from *R. rhodochrous* J1 (*58*); RRH, Co-type NHase with a high molecular weight from *R. rhodochrous* J1 (*58*); TTHA, the thiocyanate hydrolase α-subunit from *T. thioparus* (*41*); TTHB, the thiocyanate hydrolase *β*-subunit (*41*); and TTHG, the thiocyanate hydrolase *γ*-subunit (*41*). Homologous amino acid residues among the NHases are denoted with colored backgrounds (red, blue, green, and brown). The red background denotes the residues forming the active site. The residues with a blue background form networks of hydrogen bonds with hydration water molecules around the active site (see Figure 3B). The residues with a green background are the members of the aromatic cluster near the active center (see Figure 1B). The symbols # and * denote the residues engaged in intersubunit interactions and those forming the entrance channel from the bulk solvent to the active center, respectively. The secondary structure elements of Fe-type NHase from *Rhodococcus* sp. N-771 (see Figure 1) are shown in the first line. The first capital letters, H and S, in the name of the secondary structure represent α-helix and *β*-sheet, respectively. At the bottom of each panel, the number of homologous amino acid residues among the NHase family and that of identical amino acid residues with the NHase from *Rhodococcus* sp. N-771 are presented with their percentage against the total number of residues.

Recently, the primary sequence of thiocyanate hydrolase from *Thiobacillus thioparus* THI 115 has been reported (*41*). This enzyme is composed of three subunits (α-, *β*-, and *γ*-subunits). The primary sequence of the enzyme was homologous with those of the enzymes in the NHase family, and 14−32% of the primary sequence in each subunit is identical with this enzyme (Figure 7). In particular, the claw setting sequence motif (Cys-X-Leu-Cys-Ser-Cys) found in this NHase is conserved in thiocyanate hydrolase, suggesting that the coordination sphere of the active center in thiocyanate hydrolase is very similar to that in this Fe-type NHase. We also find the conservation of some of the amino acid residues stabilizing the active center with the hydration water molecules in this NHase (Figure 3). This fact leads to the idea that several hydration water molecules may be also structurally homologous between the two enzymes. This idea may be examined by analyzing the structure of thiocyanate hydrolase.

Aggregation State of NHase in Solution. Through the light scattering measurements, this study provides the first evidence that NHase exists in an equilibrium between the heterodimer and the heterotetramer in solution with a rapid exchange rate (Figure 4). The molecular weights of photoreactive NHases from *Rhodococcus* sp. N-771, N-774, and R312 have been estimated to be 60K, 70K, and 85K, respectively, by size-exclusion chromatography (*8*, *42*, *43*), despite their identical amino acid sequences (*30*, *31*, *44*). Although the protein concentrations used in these experiments are not reported, the discrepancies should be explained by the concentration-dependent aggregation of NHase molecules. Under the crystallization conditions reported so far (*16*, *24*, *28*), NHase molecules are concentrated to 5−10 mg/mL, and the equilibrium greatly shifts toward the heterotetramer dominant state. This idea is very consistent with the fact that NHases in both the active and inactive states exist as the $(\alpha\beta)_2$ heterotetramers in the crystals.

It is widely believed that both Fe-type and Co-type NHases have heterotetramer $(\alpha\beta)_2$ structure except for the high-molecular weight NHase (H-NHase) from *Rhodococcus rhodochrous* J1 (*45*) which has a higher aggregation state such as $(\alpha\beta)_{10-11}$. These results indicated that NHase exists mainly as a heterotetramer at least in several strains, including *Rhodococcus* sp. N-771 in vivo, because the amount of enzyme reaches almost 10% of the total protein in a cell. The biological meaning of tetramer formation remains unclear; however, the minimum functional unit of NHase is the $\alpha\beta$ dimer. In the formation of the heterotetramer both in vivo and in vitro, the 50 hydration water molecules probably assist the interdimer interactions by forming the networks of hydrogen bonds as observed in the crystal structure (Figure 1A). The conservation of the N-terminal residues in the β-subunit among the known NHases (Figure 7) also suggests this possibility, because the region is greatly stabilized through the formation of the heterotetramer in this Fe-type NHase.

Substrate Selection by the Entrance Channel from the Bulk Solvent to the Active Center. The substrate specificity of this Fe-type NHase catalyzing small aliphatic nitriles (*2*, *43*) is likely explained by the structures of the narrow entrance channel from the bulk solvent to the active center. On the other hand, Co-type L-NHase tends to catalyze aromatic substrates rather than aliphatic ones (*1*, *47*), and the 1,4-dioxane molecule (Figures 3A and 6C), a competitive inhibitor for this Fe-type NHase, does not inhibit the Co-type NHase with a high molecular weight from *R. rhodochrous* J1 (H-NHase) (M. Kobayashi and T. Ohkouchi, unpublished work). The Co-type NHase with a low molecular weight from *R. rhodochrous* J1 (L-NHase) lacks Leu39B in this Fe-type NHase, and H-NHase lacks Met40B (Figure 7B). These substitutions may change the structure of the channel and the substrate specificity. Therefore, we expect that the modification of the residues forming the channel may enable the novel design of NHases with the same reaction mechanism and wider substrate specificity than the wild-type NHase.

Around this channel, little appreciable structural changes are observed between the active (*28*) and the inactive states; the rms difference for all atoms forming the channel was less than 0.4 Å between the two states. To open this narrow channel, Gln90A, Phe41B, Val44B, and/or Val52B is expected to work as a gate for substrates. These residues may have the multiconformational substates as observed for Leu62 of myoglobin through a cryogenic crystal structure analysis (*46*). This idea will be further refined at the molecular level by point mutagenesis and cryogenic crystal structure analyses.

Suppression for the Photo-Reactivation of NHase Complexed with a 1,4-Dioxane Molecule after Crystallization. Through the spectroscopic (Figure 6A,B) and X-ray crystal structure analyses (Figure 6C), NHase molecules in the orthorhombic crystal are inactive even under strong light irradiation. The absorption spectrum in the 350−500 nm region was mostly followed by the excitation profiles in the resonance Raman bands originating from the Fe−NO stretching and bending region (*14*). This fact further confirms the interpretation of the absorption measurements that the NHase molecules in the crystals are in the inactive sate. The main cause of this inactivation in the crystal is that the 1,4-dioxane molecule completely prevents the escape of the endogenous NO molecule from the active center even under strong light irradiation.

In spite of the fact that the binding constant for binding of the 1,4-dioxane molecule to NHase is relatively low ($K_i = 800\ \mu$M; T. Ohkouchi et al., manuscript in preparation), the electron density map indicated that the molecule rigidly binds to the entrance channel under both the dark and light conditions. In contrast, the enzymes obtained by dissolving the crystals recovered their photo-reactivation capability (Figure 6A,B), indicating that the release of the dioxane molecule from the active center occurs in solution. These findings should be explained by that the molecular packing in the crystal prevents the dynamical motion of the entrance channel for releasing the dioxane molecule. Because the entrance channel has no significant crystal contacts, the effect is quite dynamical. Furthermore, the nearly identical structures in the entrance portions between the active and the inactive states suggested that any transient motions as described in the previous section should occur in the side chains forming the entrance.

Plausible Candidates for the Hydration Water Molecule Causing Nucleophile Attack on the Nitrile Group. Among the proposed reaction mechanisms of the Fe-type NHase (*1*, *28*, *43*), we are particularly interested in that involving direct binding of substrates to the iron atom. There are two pieces of evidence supporting the reaction mechanism. (i) Iodacetonitrile directly binds to the iron atom as reported in the crystal structure analysis for NHase in the active state (*28*), and (ii) Co−chelate complexes bind the nitrile reagent (*49*, *50*). In that mechanism, the nitrogen atom of a nitrile reagent directly binds to the non-heme iron atom after pushing out the hydroxide ion or a hydration water molecule occupying the sixth ligand site of the iron atom (*51*), and the iron atom acts as a Lewis acid in the reaction (*28*). This reaction requires a nucleophile attack of a water molecule or a hydroxide ion on the carbon atom of the nitrile group. Because the iron atom in the ferric state strongly attracts electrons of the carbon atom in the nitrile group, the carbon atom is likely to have a positive charge for accepting nucleophile attack.

The nucleophile attack of a water molecule is restricted by the constellation of protein atoms composing the active center (Figure 6C). In particular, the two post-translationally modified cysteine residues make a wall in the reaction field. Therefore, the nucleophile attack is possible only from the other side. This analysis of the hydration networks around the active center (Figure 3) suggests that significant rearrangement of hydration water molecules is difficult. Therefore, most of the hydration water molecules around the center probably reside in the positions observed in the crystal structure. The only three hydration water molecules (6, 16, and 17 in Figure 3) are the plausible candidates for a hydration water molecule causing direct nucleophile attack or transformed to hydroxide ion during the reaction, because these molecules are located within 4.2 Å of the oxygen atom of the endogenous NO molecule. However, for understanding the reaction mechanism, required are time-resolved and/or cryogenic crystal structure analyses with both the wild type and the mutated enzymes.

ACKNOWLEDGMENT

We gratefully acknowledge Dr. M. Kobayashi and Mr. T. Ohkouchi for providing us their unpublished results. We also thank Mr. M. Nakamura of Shoko Co., Ltd., for his kind help with the SEC-MALLS measurements. We also thank Prof. N. Sakabe and Dr. N. Watanabe of the Photon Factory (PF) for their help with the diffraction data collection at the PF. The diffraction data collection at the PF BL18B was carried out under an approval of the PF Program Advisory Committee. Finally, we express our gratitude to the two anonymous referees for their kind comments and suggestions in revising our manuscript.

REFERENCES

1. Kobayashi, M., and Shimizu, S. (1998) *Nat. Biotechnol. 16*, 733−736.
2. Kobayashi, M., Nagasawa, T., and Yamada, H. (1992) *Trends Biotechnol. 11*, 402−408.
3. Sugiura, Y., Kuwahara, J., Nagasawa, T., and Yamada, H. (1987) *J. Am. Chem. Soc. 109*, 5848−5850.
4. Brennan, B. A., Alms, G., Nelson, M. J., Durney, L. T., and Scarrow, R. C. (1996) *J. Am. Chem. Soc. 118*, 9144−9145.
5. Nagamune, T., Kurata, H., Hirata, M., Honda, J., Hirata, A., and Endo, I. (1990) *Photochem. Photobiol. 51*, 87−90.
6. Nakajima, T., Doi, Y., Saitoh, Y., Fujisawa, A., and Watanabe, I. (1987) *Chem. Lett. 9*, 1767−1770.
7. Scarrow, R. C., Brennan, B. A., Cummings, J. G., Jin, H., Duong, D. J., Kindt, J. T., and Nelson, M. J. (1996) *Biochemistry 35*, 10078−10088.
8. Nagamune, T., Kurata, H., Hirata, M., Honda, J., Koike, H., Ikeuchi, M., Inoue, Y., Hirata, A., and Endo, I. (1990) *Biochem. Biophys. Res. Commun. 168*, 437−442.
9. Bonnet, D., Artaud, I., Moali, C., Pétré, D., and Mansuy, D. (1997) *FEBS Lett. 409*, 216−220.
10. Honda, J., Nagamune, T., Teratani, Y., Hirata, A., Sasabe, H., and Endo, I. (1992) *Ann. N.Y. Acad. Sci. 672*, 29−36.
11. Honda, J., Teratani, Y., Kobayashi, Y., Nagamune, T., Sasabe, H., Hirata, A., and Endo, I. (1992) *FEBS Lett. 301*, 177−180.
12. Honda, J., Kandori, H., Okada, T., Nagamune, T., Shichida, Y., Sasabe, H., Ambe, F., and Endo, I. (1994) *Biochemistry 33*, 3577−3583.
13. Noguchi, T., Honda, J., Nagamune, T., Sasabe, H., Inoue, Y., and Endo, I. (1995) *FEBS Lett. 358*, 9−12.
14. Noguchi, T., Hoshino, M., Tsujimura, M., Odaka, M., Inoue, Y., and Endo, I. (1996) *Biochemistry 35*, 16777−16781.
15. Odaka, M., Fujii, K., Hoshino, M., Noguchi, T., Nagashima, S., Yohda, M., Nagamune, T., Inoue, Y., and Endo, I. (1997) *J. Am. Chem. Soc. 119*, 3785−3791.
16. Nagashima, S., Nakasako, M., Dohmae, N., Tsujimura, M., Takio, K., Odaka, M., Yohda, M., Kamiya, N., and Endo, I. (1998) *Nat. Struct. Biol. 5*, 347−351.
17. Tsujimura, M., Dohmae, N., Odaka, M., Chijimatsu, M., Takio, K., Yohda, M., Hoshino, M., Nagashima, S., and Endo, I. (1997) *J. Biol. Chem. 272*, 29454−29459.
18. Sreenivasan, U., and Axelsen, P. H. (1992) *Biochemistry 31*, 12785−12791.
19. Meyer, E. (1992) *Protein Sci. 1*, 1543−1562.
20. Levitt, M., and Park, B. (1993) *Structure 1*, 223−225.
21. Bhat, T. N., Bentley, G. A., Boulot, G., Greene, M. I., Tello, D., Dall'Acqua, W., Souchon, H., Schwarz, F. P., Mariuzza, R. A., and Poljak, R. J. (1994) *Proc. Natl. Acad. Sci. U.S.A. 91*, 1089−1093.
22. Billeter, M., Güntert, P., Luginbühl, P., and Wüthrich, K. (1996) *Cell 85*, 1057−1065.
23. Tsujimura, M., Odaka, M., Nagashima, S., Yohda, M., and Endo, I. (1996) *J. Biochem. (Tokyo) 119*, 407−411.
24. Nagamune, T., Honda, J., Cho, W.-D., Kamiya, N., Teratani, Y., Hirata, A., Sasabe, H., and Endo, I. (1991) *J. Mol. Biol. 220*, 221−222.
25. Brünger, A. T. (1992) *X-PLOR a system for X-ray crystallography and NMR*, version 3.1, Yale University Press, New Haven, CT.
26. Engh, R. A., and Huber, R. (1991) *Acta Crystallogr. A47*, 392−400.
27. Watanabe, N., Nakagawa, A., Adachi, S., and Sakabe, N. (1995) *Rev. Sci. Instrum. 66*, 1824−1826.
28. Huang, W., Jia, J., Cummings, J., Nelson, M. J., Schneider, G., and Lindqvist, Y. (1997) *Structure 5*, 691−699.
29. Bernstein, F. C., Koetzle, T. F., Williams, G. J. B., Meyer, E. F., Brice, M. D., Rodgers, J. R., Jr., Kennard, O., Shimanouchi, T., and Tasumi, M. (1977) *J. Mol. Biol. 112*, 535−542.
30. Mayaux, J., Cerbelaud, E., Soubrier, F., Faucher, D., and Pétré, D. (1990) *J. Bacteriol. 172*, 6764−6773.
31. Nojiri, M., Yohda, M., Odaka, M., Matsushita, Y., Tsujimura, M., Yoshida, T., Dohmae, N., Takio, K., and Endo, I. (1999) *J. Biochem. (Tokyo)* (in press).
32. Wyatt, P. J. (1993) *Anal. Chim. Acta 272*, 1−40.
33. Otwinowski, Z., and Minor, W. (1993) *DENZO. A Film Processing Program for Macromolecular Crystallography*, Yale University Press, New Haven, CT.
34. Hubbard, S. J., Gross, K.-H., and Argos, P. (1994) *Protein Eng. 7*, 613−626.
35. Nakamura, H. (1996) *Q. Rev. Biophys. 29*, 1−90.
36. Novotny, J., and Sharp, K. (1992) *Prog. Biophys. Mol. Biol. 58*, 203−224.
37. Parseghian, V. (1969) *Nature 221*, 844−846.
38. Otwinowski, Z., Schevitz, R. W., Zhang, R.-G., Laqson, C. L., Joachimiak, A., Marmorstein, R. Q., Luisi, B. F., and Sigler, P. B. (1988) *Nature 335*, 321−329.
39. Joachimiak, A., Haran, T. E., and Sigler, P. B. (1994) *EMBO J. 13*, 367−372.
40. Chervenak, M. C., and Toone, E. J. (1994) *J. Am. Chem. Soc. 116*, 10533−10539.
41. Katayama, Y., Matsushita, Y., Kaneko, M., Kondo, M., Mizuno, T., and Nyunoya, H. (1998) *J. Bacteriol. 180*, 2583−2589.
42. Endo, T., and Watanabe, I. (1989) *FEBS Lett. 243*, 61−64.
43. Nagasawa, T., Ryuno, K., and Yamada, H. (1986) *Biochem. Biophys. Res. Commun. 139*, 1305−1312.
44. Ikehata, O., Nishiyama, M., Horinouchi, S., and Beppu, T. (1989) *Eur. J. Biochem. 181*, 563−570.
45. Nagasawa, T., Takeuchi, K., and Yamada, H. (1991) *Eur. J. Biochem. 196*, 581−589.
46. Parak, F., Hartmann, H., Aumann, K. D., Reuscher, H., Rennekamp, G., Bartunik, H., and Steigemann, W. (1987) *Eur. Biophys. J. 15*, 237−249.
47. Komeda, H., Kobayashi, M., and Shimizu, S. (1996) *J. Biol. Chem. 271*, 15796−15802.
48. Kopf, M.-A., Bonnet, D., Artaud, I., Petre, D., and Mansuy, D. (1996) *Eur. J. Biochem. 240*, 239−244.
49. Jung, H. K., James, B., and Jik, C. (1993) *J. Am. Chem. Soc. 115*, 3618−3622.
50. Fairlie, D. P., Jackson, W. G., and Skelton, B. W. (1997) *Inorg. Chem. 36*, 1020−1028.
51. Doan, P. E., Nelson, M. J., Jin, H., and Hoffman, B. M. (1996) *J. Am. Chem. Soc. 118*, 7014−7015.
52. Brünger, A. T. (1992) *Nature 355*, 472−475.
53. Kraulis, P. J. (1991) *J. Appl. Crystallogr. 24*, 946−950.
54. Nicholls, A., Sharp, K. A., and Honig, B. (1991) *Proteins: Struct., Funct., Genet. 11*, 281−296.
55. Nishiyama, M., Horinouchi, S., Kobayashi, M., Nagasawa, T., Yamada, H., and Beppu, T. (1991) *J. Bacteriol. 173*, 2465−2472.
56. Benson, D. A., Boguski, M. S., Lipman, D. J., Ostell, J., and Ouellette, B. F. (1998) *Nucleic Acids Res. 26*, 1−7.
57. Payne, M. S., Wu, S., Fallon, R. D., Tudor, G., Stieglitz, B., Turner, I. M., Jr., and Nelson, M. J. (1997) *Biochemistry 36*, 5447−5454.
58. Kobayashi, M., Nishiyama, M., Nagasawa, T., Horinouchi, S., Beppu, T., and Yamada, H. (1991) *Biochim. Biophys. Acta 1129*, 23−33.

BI982753S